Hindawi
Mathematical Problems in Engineering
Volume 2020, Article ID 2891572, 14 pages
https://doi.org/10.1155/2020/2891572

Research Article

A Novel Neural Network-Based SINS/DVL Integrated Navigation Approach to Deal with DVL Malfunction for Underwater Vehicles

Wanli Li, Mingjian Chen, Chao Zhang, Lundong Zhang, and Rui Chen

Institute of Geospatial Information, Information Engineering University, Zhengzhou 450000, China

Correspondence should be addressed to Wanli Li; liwanli1201@hotmail.com

Received 18 February 2020; Revised 5 April 2020; Accepted 7 July 2020; Published 26 July 2020

Guest Editor: Shianghau Wu

A navigation grade Strapdown Inertial Navigation System (SINS) combined with a Doppler Velocity Log (DVL) is widely used for autonomous navigation of underwater vehicles. Whether the DVL is able to provide continuous velocity measurements is of crucial importance to the integrated navigation precision. Considering that the DVL may fail during the missions, a novel neural network-based SINS/DVL integrated navigation approach is proposed. The nonlinear autoregressive exogenous (NARX) neural network, which is able to provide reliable predictions, is employed. While the DVL is available, the neural network is trained by the body frame velocity and its increment from the SINS and the DVL measurements. Once the DVL fails, the well trained network is able to forecast the velocity which can be used for the subsequent navigation. From the experimental results, it is clearly shown that the neural network is able to provide reliable velocity predictions for about 200 s–300 s during DVL malfunction and hence maintain the short-term accuracy of the integrated navigation.

1. Introduction

The ocean covers 71% of the surface of the Earth. It is rich in biological resource and minerals resource. Underwater vehicles, including remotely operated vehicles (ROVs) and autonomous underwater vehicles (AUVs), are widely used in the exploration of the ocean. However, the lack of reliable navigation techniques is still a key fact which limits the application of the underwater vehicles. Although Global Navigation Satellite System (GNSS) is widely used in surface and air navigation [1], its signals rapidly attenuate in water. The acoustic navigation systems [2], such as Long Baseline (LBL) and Ultra Short Baseline (USBL), have a limited range. For example, the 12 kHz LBL typically operates at up to 10 km ranges [3]. Strapdown Inertial Navigation System (SINS), which is able to provide complete navigation parameters, such as position, velocity, and attitude, is usually employed in autonomous underwater navigation. However, as the positioning errors of the SINS increase with time, an external aiding sensor is necessary.

Based on Doppler Effect, the Doppler Velocity Log (DVL) is able to provide velocity measurements relative to the seafloor. It is regarded as one of the most potential aiding sensors which are able to limit the error growth of SINS [4, 5]. However, the DVL provide velocities in the Doppler instrumental frame, but not the geodetic frame. There are still challenges in DVL aided integrated navigation. For example,, misalignments between the SINS body frame and Doppler instrumental frame will occur during manufacture [6]. Therefore, a calibration process is usually required before conducting a mission [7, 8]. Even so, the position error of SINS/DVL will accumulate without any external position observations. Furthermore, the azimuth error of the integrated navigation shows slow convergence in the case of DVL aiding. Fast SINS in-motion initial alignment is also a challenge issue which has aroused great attention [9].

In addition, DVL has a limited maximum range. Table 1 shows the specifications of the DVLs [10] produced by Teledyne RD Instruments, Inc. As can be seen from the table, DVL working at a higher operating rate can provide more accurate velocity measurements, whereas its maximum range is smaller and vice versa. In the case that the acoustic wave emitted by the DVL cannot reach the seafloor, the DVL will work in the mode of water-tracked, which provides water reference velocities, or fail to provide velocities.

SINS/DVL integrated is typically accomplished by using a Kalman filter (KF), which fuses the data from the SINS and

Table 1: Specifications of the RDI workhorse navigator Doppler Velocity Log.

Parameter item	WHN 300	WHN 600	WHN 1200
Long-term accuracy	±0.4%V ± 0.2 cm/s	±0.2%V ± 0.1 cm/s	±0.2%V ± 0.1 cm/s
Operating rate	300 kHz	600 kHz	1200 kHz
Maximum range	200 m	90 m	25 m
Velocity range	±10 m/s	±10 m/s	±10 m/s

the DVL. Therefore, the accuracy of the DVL measurements is of vital importance in optimally estimating the subsequent navigation solutions. In [11], the authors proposed a pretreatment method for the velocity of DVL based on the motion constraint of underwater vehicles. It is able to restrain random noise in the DVL. Adaptive Kalman filter (AKF) is also regarded as an effective approach to deal with the accuracy decrease of the DVL [12, 13]. SINS/DVL integrated navigation, in case that only partial DVL measurements are available, is also investigated. In [14, 15], tightly coupled navigation structures are proposed to deal with the situation that DVL has fewer than three beam measurements.

Under certain conditions, such as sailing across sea creatures or the DVL exceeds its maximum measuring range, the DVL will fail to maintain bottom-lock and provide velocity updates [16, 17]. To circumvent this problem, Tal et al. [18] derived an extended loosely coupled (ELC) approach which is able to provide virtual vehicle velocity by using partial raw data of the DVL and additional information. In [19], the authors proposed a hybrid approach to forecast the measurements of the DVL while it malfunctions. The current and past velocities obtained from SINS are taken as the predictor's inputs. In this paper, we proposed a neural network-based approach to predict the body frame velocity when DVL is unavailable. Related methodologies in similar situations can be found in the literature on SINS/GNSS integrated navigation [20–22]. The main idea of these approaches is to build the map between SINS measurements (angular rate, specific force, velocity, position, and so forth) and GNSS measurements [21]. If the GNSS signals are available, the neural network is trained by the SINS and GNSS measurements. Once the outages of the GNSS happen, the virtual GNSS measurements can be obtained by the well trained neural network. Therefore, it is able to maintain the short-term stability of the SINS/GNSS integration. Inspired by these works, a nonlinear autoregressive exogenous (NARX) neural network model, which is able to forecast the velocity during the DVL malfunction, is constructed. The NARX neural network has been widely used in time series forecasting [23]. The prediction of the velocity can also be regarded as a time series forecasting problem. When DVL is available, the body frame velocity and its increment obtained from the SINS and DVL are collected to train the neural network. Once DVL is unavailable, the velocity forecasted by the well trained neural network is utilized to assist the SINS and hence maintain the accuracy of the integrated navigation.

The rest of this paper is organized as follows. Section 2 is devoted to the presentation of the SINS/DVL integrated navigation scheme. Both the SINS error dynamics model and the DVL error model are derived. Section 3 gives the algorithmic description of the neural network-based SINS/DVL integrated navigation scheme. In Section 4, the performance of the proposed algorithm is evaluated with ship-mounted experimental data collected in the Yangtze River. Conclusions are drawn in Section 5.

2. SINS/DVL Integrated Navigation

Figure 1 shows the structure of the SINS/DVL integration. Normally, the SINS is consisted of three orthogonal gyroscopes and three orthogonal accelerometers, which are able to provide angular rate and specific force in the SINS body frame (denoted as b). With these measurements, the navigation solutions including position, attitude, and velocity can be obtained. The DVL provides velocity in the Doppler instrumental frame (denoted as d). To match the velocity of SINS, firstly, it should be transformed into the body frame with alignment calibration parameters. Then, the DVL velocity can be transformed into the navigation frame (denoted as n, local-level frame, and its orientation is north-east-sown (NED)) with the attitude of the SINS. As a velocity matching integration scheme, the velocities of the DVL and SINS in the navigation frame are chosen as the input of the Kalman Filter. With the estimation of the Kalman Filter, the navigation solutions can be reset and the sensor errors such as gyro bias and accelerometer bias can be corrected. As can be seen from Figure 1, with a feedback scheme, the navigation errors of the SINS, such as attitude error and velocity error, are compensating each Kalman filter cycle.

2.1. SINS Error Dynamics Model. Due to the inherent biases (gyro bias and accelerometer bias) of the SINS, the position error, attitude error, and the velocity error accumulate with time. It is known to us that, in the case of velocity matching integrated navigation, the position error is unobservable. Therefore, the position error is abandoned to be chosen as a state of the integration. The velocity and attitude error propagation process of the SINS can be described as follows [7]:

$$\delta\dot{v}^n = [f^n\times]\phi - (2\omega_{ie}^n + \omega_{en}^n)\times\delta v^n + C_b^n\nabla, \tag{1}$$

$$\dot{\phi} = -(\omega_{ie}^n + \omega_{en}^n)\times\phi + (\delta\omega_{ie}^n + \delta\omega_{en}^n) - C_b^n\varepsilon, \tag{2}$$

where the subscript n denotes the components described in the navigation frame. δv^n is the velocity error. ϕ is the attitude error. f^n is the specific force in the navigation frame. C_b^n is the direction cosine matrix of the body frame to the navigation frame. ω_{ie}^n denotes the angular rate of the Earth frame e relative to the inertial frame i. ω_{en}^n is the angular rate of the navigation frame relative to the Earth frame. ∇ and ε are the biases of the gyro and the accelerometer in the body

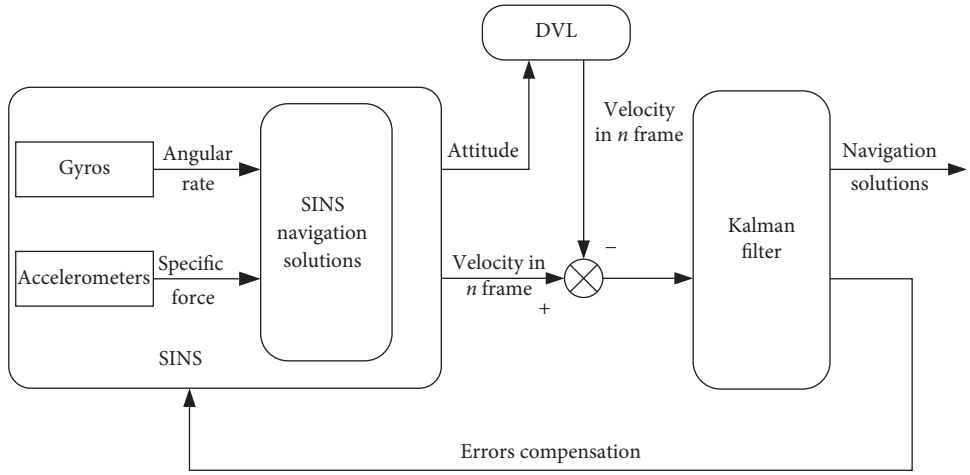

Figure 1: SINS/DVL integrated navigation structure.

frame, respectively. In SINS/DVL integration, ∇ and ε are usually modeled as random constants:

$$\dot{\nabla} = 0, \tag{3}$$

$$\dot{\varepsilon} = 0. \tag{4}$$

The error states of the SINS are chosen as follows:

$$x = \left[\delta v_N \;\; \delta v_E \;\; \delta v_D \;\; \phi_N \;\; \phi_E \;\; \phi_D \;\; \nabla_x \;\; \nabla_y \;\; \nabla_z \;\; \varepsilon_x \;\; \varepsilon_y \;\; \varepsilon_z \right]. \tag{5}$$

The SINS error dynamics model can be expressed as follows:

$$\dot{x} = Fx + w, \tag{6}$$

where w is a zeros-mean Gaussian white noise which is determined by the accuracy of the gyros and accelerometers. F is the state transformation matrix constructed according to equations (1)–(4). It can be given as follows:

$$F = \begin{bmatrix} F_{11} & F_{12} & C_b^n & 0_{3\times3} \\ F_{21} & F_{22} & 0_{3\times3} & -C_b^n \\ 0_{3\times3} & 0_{3\times3} & 0_{3\times3} & 0_{3\times3} \\ 0_{3\times3} & 0_{3\times3} & 0_{3\times3} & 0_{3\times3} \end{bmatrix}, \tag{7}$$

where

$$F_{11} = \begin{bmatrix} \dfrac{v_D}{R_N + h} & -2\omega_{ie}\sin L - 2\dfrac{v_E tgL}{R_E + h} & \dfrac{v_N}{R_N + h} \\ 2\omega_{ie}\sin L + 2\dfrac{v_E tgL}{R_E + h} & \dfrac{v_D + v_N tgL}{R_E + h} & 2\omega_{ie}\cos L + \dfrac{v_E}{R_E + h} \\ -2\dfrac{v_N}{R_N + h} & -2\omega_{ie}\cos L - \dfrac{v_E}{R_E + h} & 0 \end{bmatrix}, \tag{8}$$

whereR_E and R_N are the transverse radius and meridian radius of the Earth, respectively. L is the latitude. h denotes the altitude. ω_{ie} is the Earth's rotation rate.v_N, v_E, and v_D are the velocity in the north, east, and down direction, respectively.

$$F_{12} = \begin{bmatrix} 0 & -f_D & f_E \\ f_D & 0 & -f_N \\ -f_E & f_N & 0 \end{bmatrix}, \tag{9}$$

where f_N, f_E, and f_D are the specific force in the navigation frame. Also,

$$F_{21} = \begin{bmatrix} 0 & \frac{1}{R_E + h} & 0 \\ -\frac{1}{R_N + h} & 0 & 0 \\ 0 & \frac{tgL}{R_E + h} & 0 \end{bmatrix}, \tag{10}$$

$$F_{22} = \begin{bmatrix} 0 & -\omega_{ie} \sin L - \frac{V_E tgL}{R_E + h} & \frac{V_N}{R_N + h} \\ \omega_{ie} \sin L + \frac{V_E tgL}{R_E + h} & 0 & \omega_{ie} \cos L + \frac{V_E}{R_E + h} \\ -\frac{V_N}{R_N + h} & -\omega_{ie} \cos L - \frac{V_E}{R_E + h} & 0 \end{bmatrix}. \tag{11}$$

2.2. DVL Error Model. The velocity of DVL can be transformed into the navigation frame as follows:

$$\tilde{v}_d^n = \tilde{C}_b^n C_d^b v_d, \tag{12}$$

where v_d is the velocity of DVL in the Doppler instrumental frame d. C_d^b is the alignment matrix which presents the transformation of the Doppler instrumental frame to the body frame b; it can be presented as follows:

$$C_d^b = I_{3\times3} - \theta\times, \tag{13}$$

where $I_{3\times3}$ is a 3×3 identity matrix and $\theta\times$ denotes the skew matrix of the misalignments between the DVL and the SINS. It can be obtained by calibration [7, 8]. $\tilde{C}_b^n$ is the direction cosine matrix in error; it can be obtained by

$$\tilde{C}_b^n = [I_{3\times3} - \phi\times] C_b^n, \tag{14}$$

where $\phi\times$ denotes the skew matrix of the attitude error ϕ. Substituting (14) into (12), it yields

$$\begin{aligned} \tilde{v}_d^n &= [I_{3\times3} - \phi\times] C_b^n C_d^b v_d, \\ &= C_b^n C_d^b v_d + \left[\left(C_b^n C_d^b v_d\right)\times\right]\phi, \\ &= v^n + \delta v_d. \end{aligned} \tag{15}$$

The velocity of the SINS in error can be modeled as

$$\tilde{v}_{\text{SINS}}^n = v^n + \delta v^n. \tag{16}$$

Differencing the velocity of the SINS and DVL in the navigation frame, there exists

$$\begin{aligned} \tilde{v}_{\text{SINS}}^n - \tilde{v}_d^n &= \left(v^n + \delta v^n\right) - \left(v^n + \delta v_d^n\right) \\ &= \delta v^n - \left[\left(C_b^n C_d^b v_d\right)\times\right]\phi. \end{aligned} \tag{17}$$

It can be represented by the following equation:

$$z = \tilde{v}_{\text{SINS}}^n - \tilde{v}_d^n = Hx + \eta, \tag{18}$$

where η is a zeros-mean Gaussian white noise which is determined by the accuracy of the DVL. H can be obtained from equation (17) as follows:

$$H = \left[\, I_{3\times3} \quad \left(C_b^n C_d^b v_d\right)\times \quad 0_{3\times6} \,\right]. \tag{19}$$

2.3. Standard Kalman Filter. The integrated navigation model described by equation (6) and equation (18) can be discretized as follows:

$$\begin{cases} X_k = \Phi_{k,k-1} X_{k-1} + W_k, \\ Z_k = H_k X_{k-1} + V_k, \end{cases} \tag{20}$$

where X_k is the state vector, Z_k is the measurement vector, $\Phi_{k,k-1}$ is the state transition matrix, and H_k is the measurement matrix. W_k and V_k are uncorrelated zeros-mean Gaussian white noise and their conversances can be given as follows:

$$E[W_k W_i] = \begin{cases} Q_k & k = i, \\ 0 & k \neq i, \end{cases} \tag{21}$$

$$E[V_k V_i] = \begin{cases} R_k & k = i, \\ 0 & k \neq i, \end{cases} \tag{22}$$

$$E[V_k W_i] = 0, \quad \forall k, i. \tag{23}$$

Kalman filter is able to estimate the state vector from the measurement vector in an optimum way. It is consisted of time update and measurement update. If there are no DVL measurements, time update is employed to predict the state vector as follows [11]:

$$\widehat{X}_{k,k-1} = \Phi_{k,k-1}\widehat{X}_{k-1}, \tag{24}$$

$$P_{k,k-1} = \Phi_{k,k-1}P_{k-1}\Phi_{k,k-1}^{T} + Q_{k-1}, \tag{25}$$

where $\widehat{X}_{k,k-1}$ is the predicted state vector and $P_{k,k-1}$ is the predicted covariance matrix of $\widehat{X}_{k,k-1}$. Once the DVL measurement is available, the measurement update can be accomplished as follows:

$$\widehat{X}_k = \widehat{X}_{k,k-1} + K_k\left[Z_k - H_k\widehat{X}_{k,k-1}\right], \tag{26}$$

$$K_k = P_{k,k-1}H_k^T\left[H_kP_{k,k-1}H_k^T + R_k\right]^{-1}, \tag{27}$$

$$P_k = \left[I - K_kH_k\right]P_{k,k-1}\left[I - K_kH_k\right]^T + K_kR_kK_k^T, \tag{28}$$

where K_k is the Kalman Filter gain. Then, the navigation solutions of the SINS/DVL integration can be updated by the estimation of the state vector $\widehat{X}_k$.

3. Neural Network-Based Integrated Navigation Structure

As mentioned in Section 1, the DVL may fail to provide velocity in some situations. To deal with this problem, a neural network-based approach is proposed. The main idea is to forecast the velocity measurements by neural network during DVL malfunction. And hence the subsequent integrated navigation can be conducted with the predictions. Since the velocity of the DVL is in the Doppler instrumental frame d, it should be transformed into the body frame by the alignment matrix C_d^b before integration as follows:

$$v^b = C_d^b v^d. \tag{29}$$

The neural network will predict the body frame velocity directly. In this paper, a nonlinear autoregressive exogenous neural network is employed [24]. That is, the current value of a time series can be forecasted by two series: the previous values of the same series and the current and previous values of the driving series. The driving series is the series that influences the series of interest.

The NARX model can be described as follows [25]:

$$y_{k+1} = M\begin{pmatrix} y_k & y_{k-1} & \cdots & y_{k-m} & x_{k+1} \\ x_k & x_{k-1} & \cdots & x_{k-m} & \end{pmatrix}, \tag{30}$$

where $M(\cdot)$ is the mapping function of the neural network, x_k is the value of the driving series at time k, and y_k is the value of the target series at time k. Obviously, the body frame velocity sequence is the target time series. Considering that the body frame velocity increment sequence of SINS can also indicate the change of the velocity, it is chosen as the driving series. The velocity increment of the SINS in n-frame u^n can be obtained by the two-sample iteration algorithm [26]. The velocity increment of the SINS in b frame during each DVL update cycle can be given as follows:

$$\Delta v_k^b = \sum_{i=1}^{N} C_n^b\left(t_{k-1} + i \times T\right)u^n\left(t_{k-1} + i \times T\right), \tag{31}$$

where T is the SINS update cycle and N denotes the amount of SINS update during each DVL update cycle.

The variables of the mapping function, which are initially stochastic, can be fine-tuned in the training process. The multilayer perceptron network is employed to perform the approximation and its configuration is shown in Figure 2. Considering that the training of the neural network requires a lot of data, a light-weight neural network model is employed. Therefore, the employed model is easy for training and fine-tuning, and no massive training data is required. The network is composed of three layers: input layer, hidden layer, and output layer. Both the body frame velocity and the velocity increment have three dimensions, so there are six attributes of the input. The velocities of the previous two steps are also adopted as the input of the network. There are ten neurons in the hidden layer. The final output of the network is the predicted body frame velocity which is a three-dimensional vector. The Levenberg–Marquardt (LM) optimization method is adopted as the training function for the network [27].

The structure of the improved SINS/DVL integration is shown in Figure 3. When the DVL is available, the SINS is integrated with the DVL to get navigation solutions. Meanwhile, the neural network is trained by the velocity and velocity increment in b frame. The driving series can be obtained continuously by the SINS:

$$x_k = \Delta v_k^b,\ k = 1, 2, \cdots, m, \tag{32}$$

where the velocity increment Δv_k^b can be obtained from equation (31). The target series can be acquired from equation (29) with DVL measurements as follows:

$$y_k = v_k^b,\ k = 1, 2, \cdots, m. \tag{33}$$

Once the DVL fails, the velocity in b frame can be predicted by the well trained network. However, with the DVL measurements, the network is able to predict only one step ahead. Therefore, the subsequent integrated navigation is conducted as follows:

Step 1: predict the velocity in b frame one step ahead with the input time series of current and the previous two steps.

Step 2: update the SINS navigation solutions and the velocity increment in b frame with the SINS raw data.

Step 3: conduct the SINS/DVL integrated navigation and update navigation solutions. Update the driving series with the velocity increment obtained by Step 2. Update the target series with the prediction obtained by Step 1.

Step 4: go to Step 1 until the integrated navigation is finished

4. Experimental Results and Discussion

4.1. Test Configuration. The ship-mounted experimental data were collected to evaluate the performance of the proposed algorithm. The trial was carried out in the Yangtze River. The equipped instruments include a navigation grade

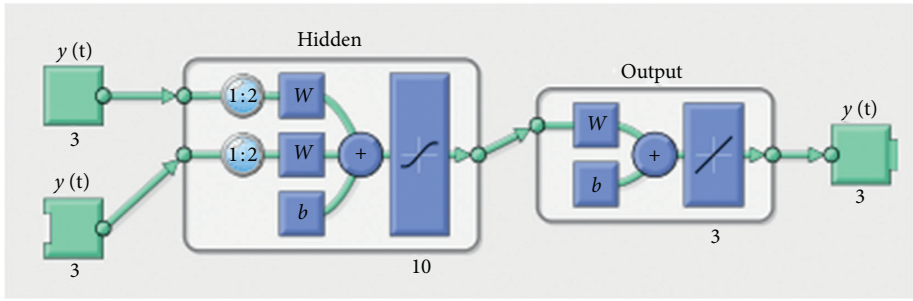

Figure 2: NARX generated by MATLAB R2014a.

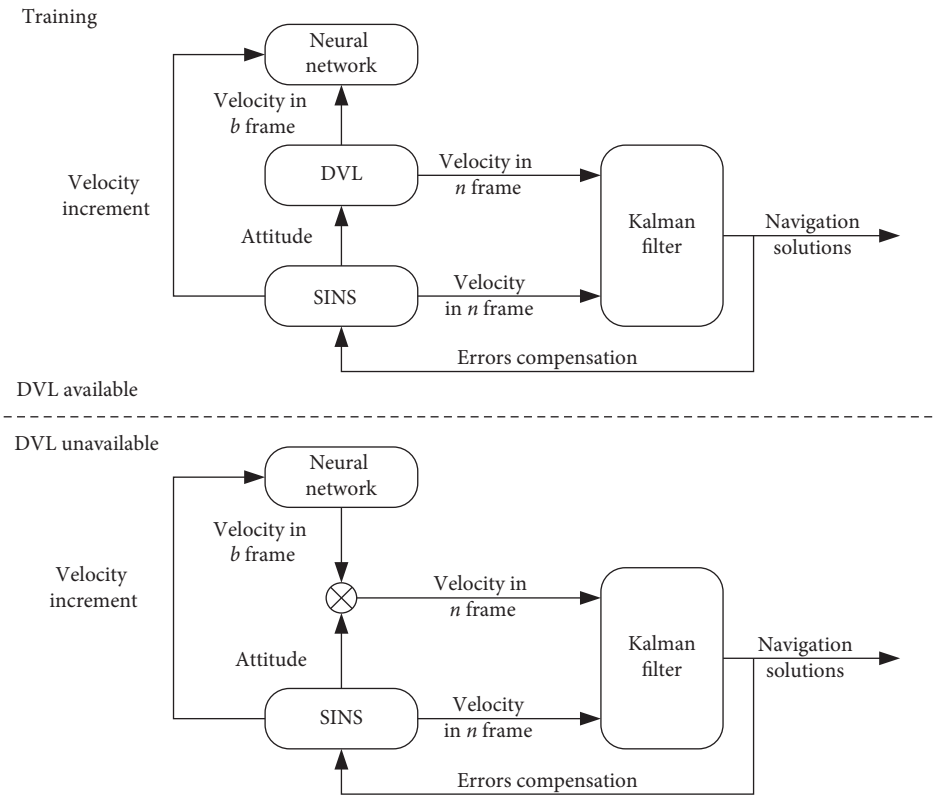

Figure 3: Structure of the improved SINS/DVL integration.

SINS, a bottom-locked DVL, and a NovAtel GPS receiver. The specifications of the SINS and DVL are shown in Tables 2 and 3, respectively.

4.2. Performance Evaluation of the SINS/DVL Integration. During the test, the ship sailed up to about 30 kilometers at the speed of around 9 knots (approximately 6600 s). From the experimental data, it is shown that the GPS receiver was able to provide credible position and velocity measurements during the whole test. Therefore, the integrated navigation results, including position, velocity, and attitude from SINS/GPS, can be used as the benchmark to compare with the SINS/DVL integration. Before integrated navigation, an initial alignment of SINS was conducted. The trajectories obtained from SINS/GPS and SINS/DVL are shown in

Table 2: SINS specifications.

Parameter item	Gyroscope	Accelerometer
Bias	$<0.02^{\circ}/h(1\sigma)$	$<5\times10^{-5}$g (1σ)
Update rate	200 Hz	200 Hz
Bias stability	<30 ppm	<50 ppm
Dynamic range	$\pm200^{\circ}$(s)	±15 g

Table 3: DVL specifications.

Parameter item	
Velocity accuracy	±0.5%V ± 0.5 cm/s
Update rate	1 Hz
Operating rate	300 kHz
Bottom-locked range	300 m
Dynamic range	−10 knot~20 knot

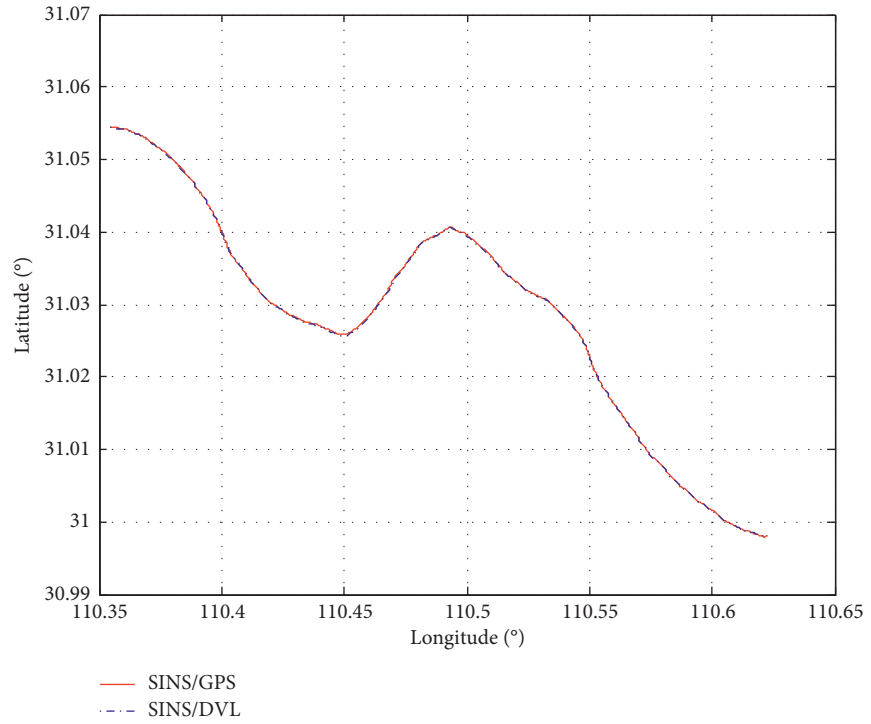

Figure 4: Trajectories obtained from the SINS/GPS and the SINS/DVL.

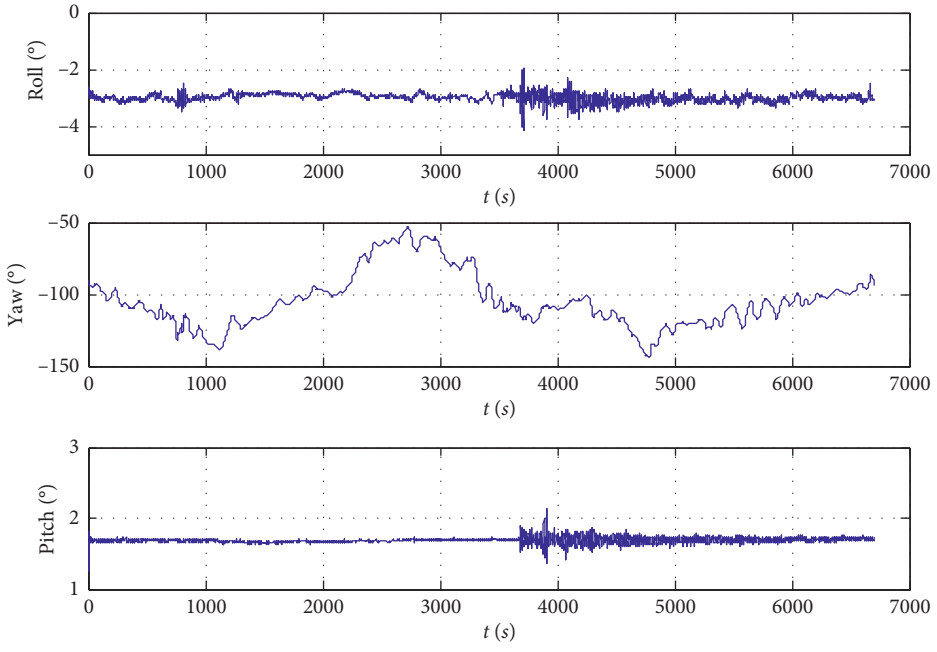

Figure 5: The attitude of the ship.

Figure 4. Figure 5 shows the changing of attitude. Figures 6 and 7 show the velocities in the navigation frame and Doppler instrumental frame, respectively. As can be seen from the figures, the roll and the pitch of the ship remain around −3° and 1.7°, respectively. The heading and the velocity of the ship vary slowly. The AUVs usually operate within a low dynamics range. It may fit the real motion of the AUVs, such as submarines. As can be seen from Figure 4, the two trajectories closely match each other. The error curve of the position is shown in Figure 8. And the final position error of the SINS/DVL integration is about 28 meters, which is less than 1% of the distance travelled. Predictably, as long as external position observations are unavailable, the position error will accumulate with time.

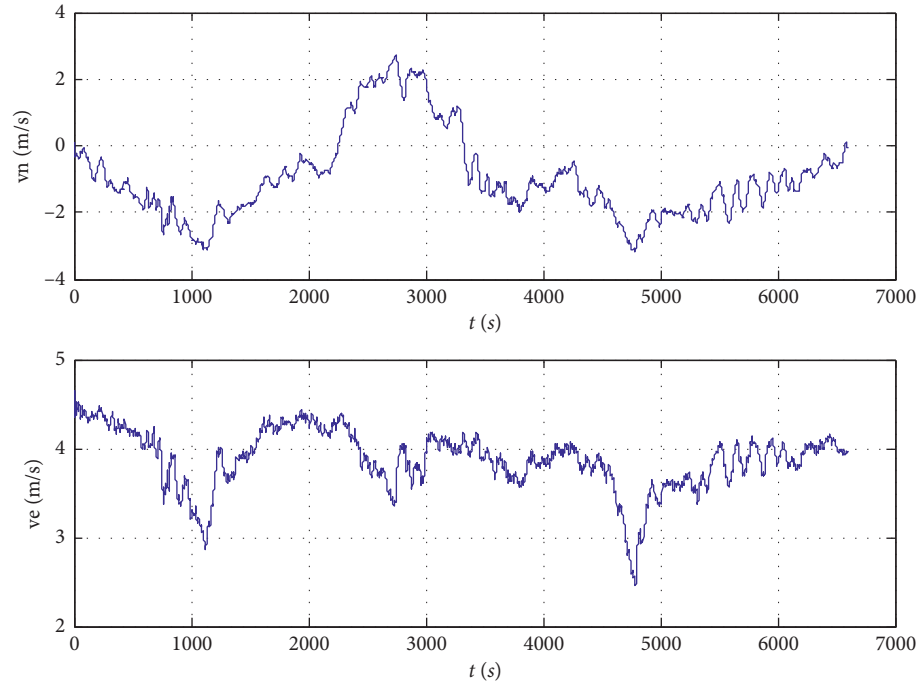

Figure 6: The velocity of the ship in the navigation frame.

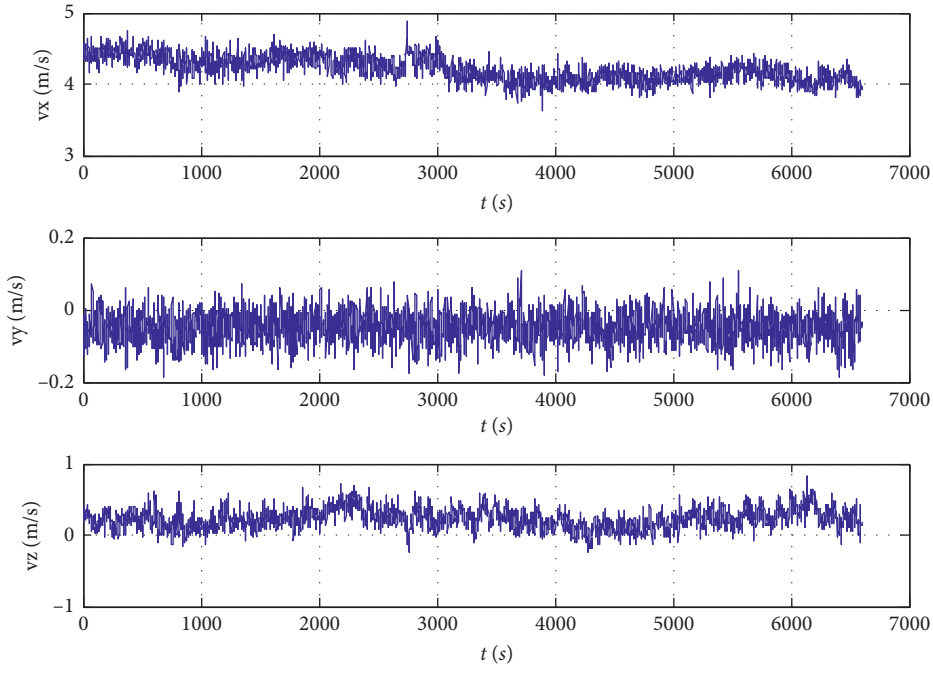

Figure 7: The DVL measurements during the experiment.

As the DVL provides the velocity measurements in the Doppler instrumental frame but not geodetic frame, it leads to the slow convergence of the heading error and INS measurement errors (the gyro biases and the accelerometer biases). In addition, the AUVs usually operate within a low dynamics range, which makes this problem more serious. Both the gyro and the accelerometer biases in the up direction cannot be estimated as reliable. Therefore, the open loop is adopted to estimate the INS biases [28]. Misalignments of the SINS/DVL are shown in Figure 9. The misalignments converge with time. However, the heading error converged slower than the roll error and the pitch error. It oscillates at the beginning and then converges. From the partial magnification of Figure 9, the heading error remains

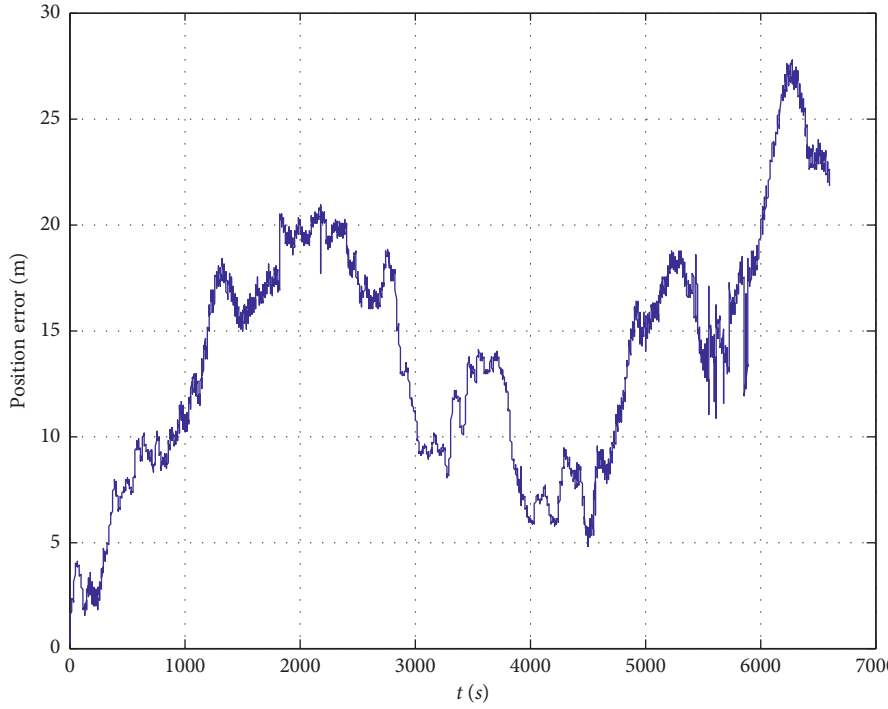

Figure 8: Position error of the SINS/DVL.

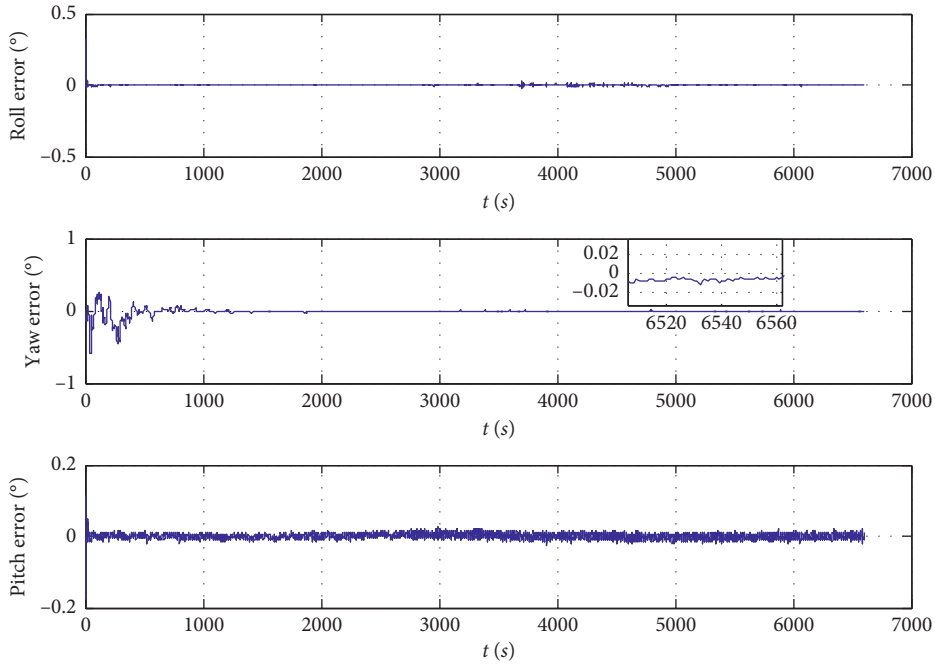

Figure 9: Misalignments of the SINS/DVL.

around 0.01° finally. It is known that DVL provides velocity measurements in the Doppler instrumental frame. And it leads to the slow convergence of the heading. Figure 10 shows the velocity error in the north and east direction, respectively. As a velocity-aided integration, the velocity errors of SINS/DVL show fast convergence.

4.3. Validation of the Proposed Neural Network-Based Algorithm. A test was designed to evaluate the performance of the proposed neural network-based algorithm. In practical use, the flag denoting whether the DVL is available has been set. As the DVL is available during the whole mission, it is assumed that DVL is unavailable after 4000 s. And the

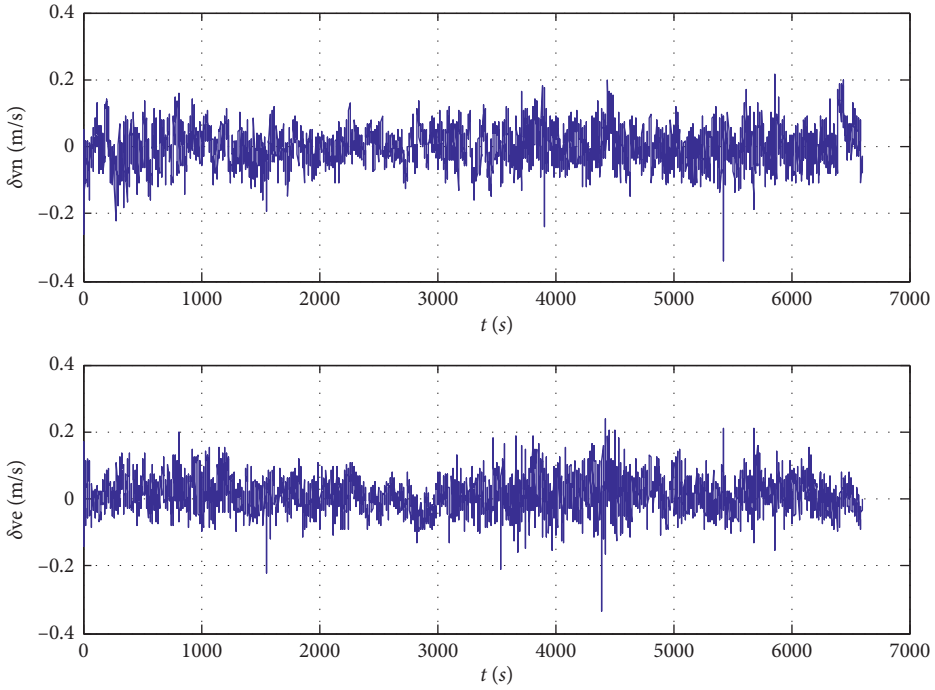

Figure 10: Velocity errors of SINS/DVL in the navigation frame.

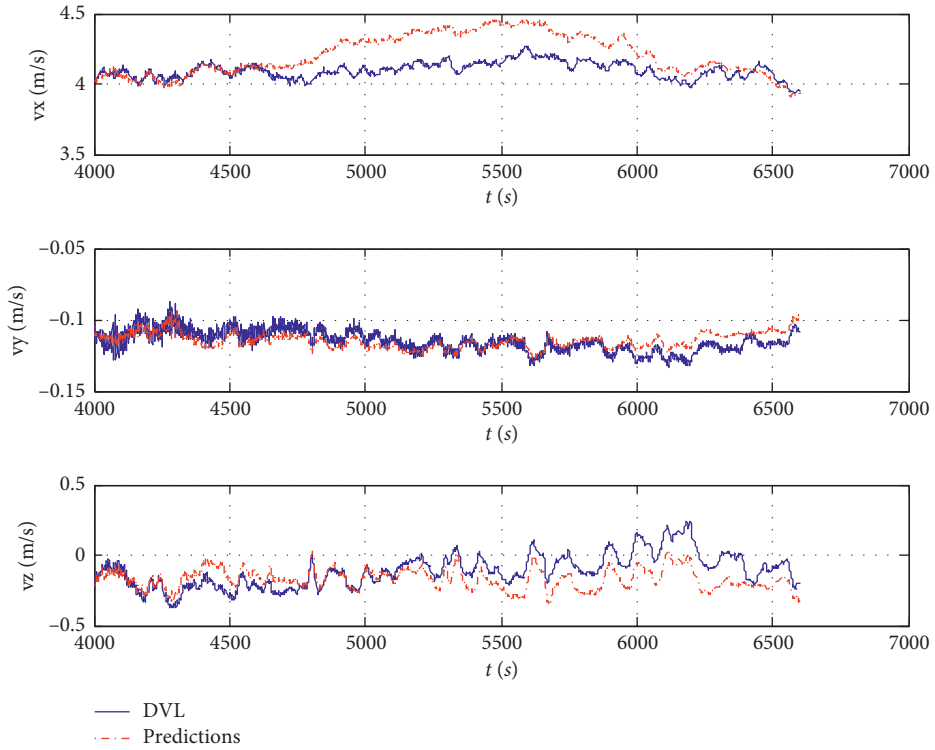

Figure 11: Body frame velocity obtained from the DVL and the neural network.

former data was employed to train the neural network. Therefore, the network is able to forecast the body frame velocity which can be used in the subsequent integrated navigation.

The body frame velocity obtained by DVL can be regarded as the actual value. Figure 11 compares the body frame velocity from the DVL and the network. As can be seen from the figure, the predicted values match well with

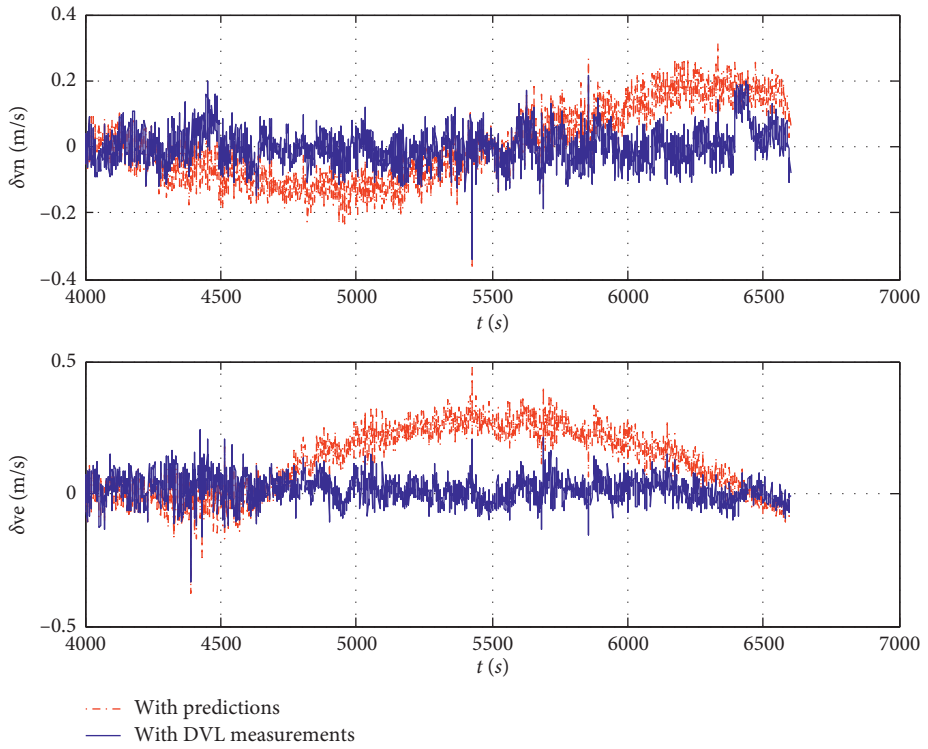

Figure 12: Velocity errors of SINS/DVL in the navigation frame.

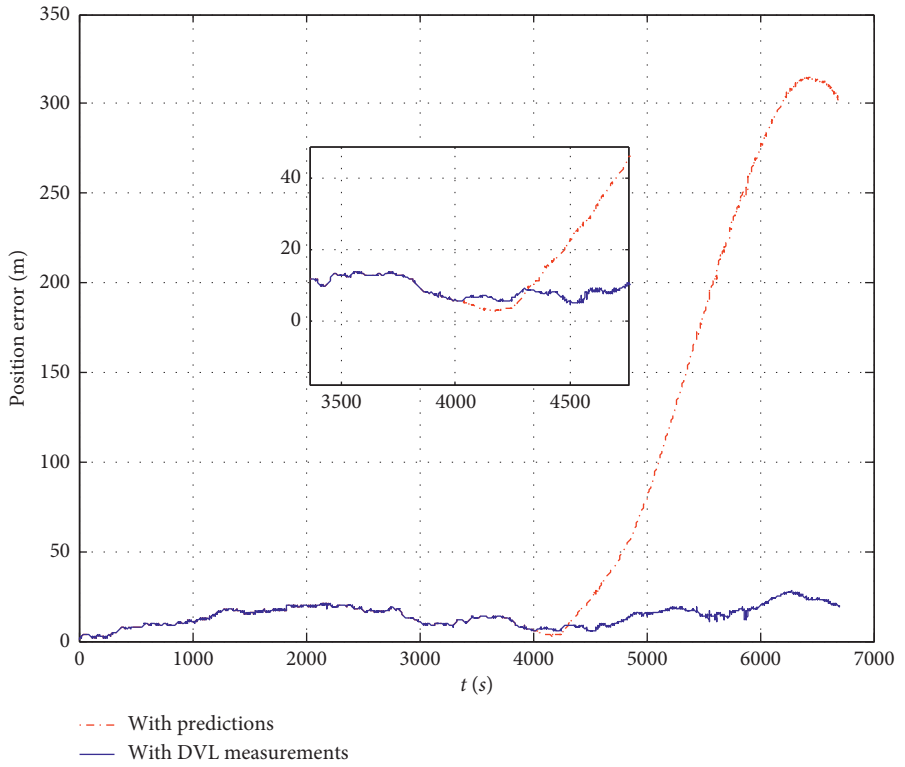

Figure 13: Position errors of the SINS/DVL.

the real value at the beginning, especially the first 200 s–300 s. However, with the increase of time, the difference of the velocities becomes larger.

Compared with the experimental results that DVLs are always available, Figures 12 and 13 show the velocity errors and the position errors of the integrated navigation,

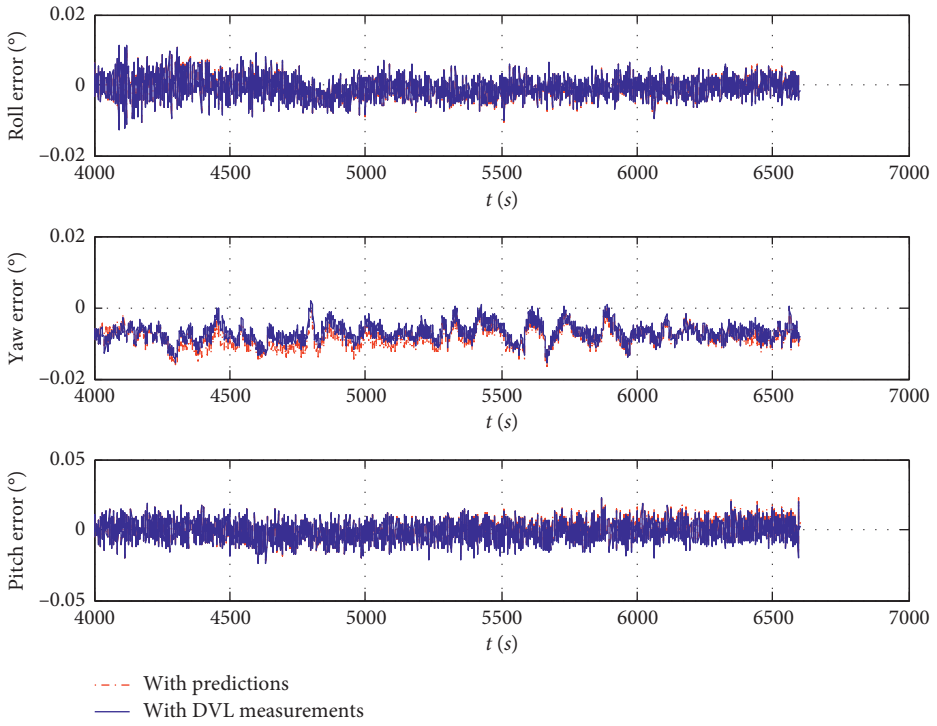

Figure 14: Attitude errors of the SINS/DVL.

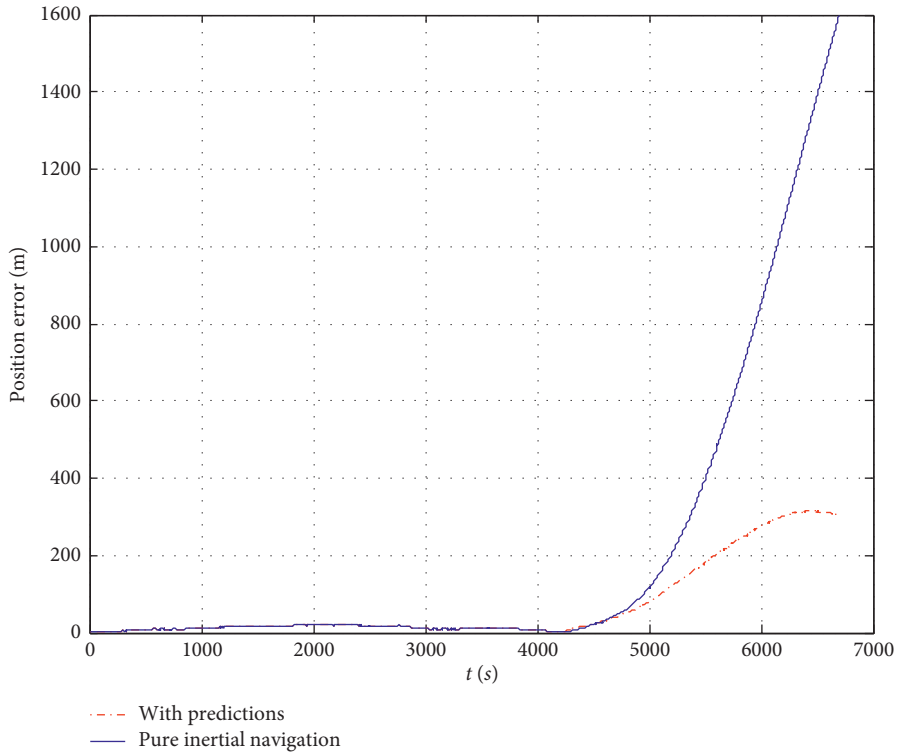

Figure 15: Comparison of the position errors.

respectively. It is shown in Figure 12 that the velocity error of the SINS/DVL with DVL measurements remains around zero. And the velocity error of the SINS/DVL with the predictions also remains around zero at the beginning. However, it diverges with the increase of time. Obviously, the divergence of the velocity error will lead to the growth of the position error. As can be seen from the partial magnification of Figure 13, the positioning error of the SINS/DVL

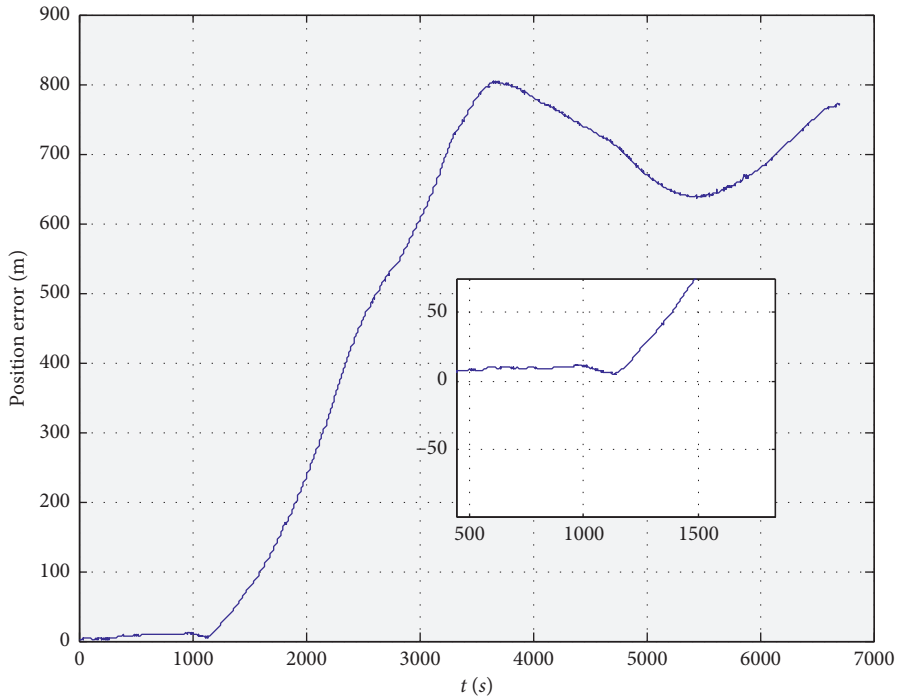

Figure 16: Position error of the SINS/DVL with 1000 s training data.

with predictions is extremely close to that with DVL measurements during the first 200 s–300 s and then increases with time. From the experimental results presented above, it is clearly shown that the proposed neural network-based approach is able to deal with short-term (approximately 200 s–300 s) malfunction of the DVL. However, as the predicting error of the neural network becomes larger, the positioning error of SINS/DVL will increase gradually.

Figure 14 shows the attitude errors of the SINS/DVL. As can be seen from the figure, the influence of the inaccurate velocity predictions on the attitude is not that obvious. The error curves still match well with each other. The final heading error of the SINS integrated with the predictions is around 0.01°. However, it is expected that the difference of the attitude errors will become larger if a low accuracy SINS is employed.

In practical use, when the DVL output is unavailable, the SINS work solely. A comparison has been done by comparing the position error of pure inertial navigation and SINS integrated with DVL predictions. It is clearly shown in Figure 15 that the SINS/DVL integration with DVL predictions is able to reduce the error growth while the position error of the pure inertial navigation increases rapidly. This provides another confirmation to the superiority of the proposed method.

Experiments have also been done by intentionally reducing the amount of the training data. Figure 16 shows the position error of the SINS/DVL with 1000s training data. From partial magnification of the figure, it is found that the SINS/DVL integration is able to maintain accuracy for only about 100 s–150 s. It is shown that, once the amount of the training data is reduced, the accuracy of the predictions will be reduced, too.

5. Conclusions

To deal with the problem of DVL malfunction in SINS/DVL integrated navigation, a neural network-based approach is proposed. When the DVL is available, the measurements from the SINS and DVL are employed to train the network. Once the DVL fails, the well trained network is able to forecast the velocity which can be used in the subsequent integrated navigation. From the experimental results, the following conclusions can be drawn.

(1) With a navigation grade SINS and a DVL, the trained neural network is able to provide credible velocity predictions. But the error of the prediction will increase with time gradually.

(2) With the predicted velocity series from the well trained network, the SINS/DVL integration is able to maintain accuracy for about 200 s–300 s. Therefore, the proposed approach is capable of dealing with DVL short-term malfunction.

(3) If the amount of training data is reduced, the accuracy of DVL predictions may decrease, too.

In this paper, a navigation grade SINS is employed in the experiment. Further investigation is still needed to determine whether this approach is suitable for low cost inertial navigation systems.

Data Availability

The data used to support the findings of this study is owned by the Information Engineering University and so cannot be made freely available. Access to these data will be considered by the author upon request, with the permission of the

Research Management Department of Information Engineering University.

Conflicts of Interest

The authors declare no conflicts of interest.

Acknowledgments

This research was supported in part by the National Natural Science Foundation of China (Nos. 41674027 and 41604011).

References

[1] D. H. Won, E. Lee, M. Heo, S. Sung, J. Lee, and Y. J. Lee, "GNSS integration with vision-based navigation for low GNSS visibility conditions," *GPS Solutions*, vol. 18, no. 2, pp. 177–187, 2014.

[2] T. Zhang, L. Chen, and Y. Li, "AUV underwater positioning algorithm based on interactive assistance of SINS and LBL," *Sensors*, vol. 16, no. 42, 2016.

[3] J. C. Kinsey and L. L. Whitcomb, "In situ alignment calibration of attitude and Doppler sensors for precision underwater vehicle navigation: theory and experiment," *IEEE Journal of Oceanic Engineering*, vol. 32, no. 2, pp. 286–299, 2007.

[4] A. Karmozdi, M. Hashemi, and H. Salarieh, "Design and practical implementation of kinematic constraints in inertial navigation system-Doppler velocity log (INS-DVL)-based navigation," *Navigation*, vol. 65, no. 4, pp. 629–642, 2018.

[5] L. Paull, S. Saeedi, M. Seto, and H. Li, "AUV navigation and localization: a review," *IEEE Journal of Oceanic Engineering*, vol. 39, no. 1, pp. 131–149, 2014.

[6] X. Pan and Y. Wu, "Underwater Doppler navigation with self-calibration," *Journal of Navigation*, vol. 69, no. 2, pp. 295–312, 2016.

[7] W. Li, L. Zhang, F. Sun, L. Yang, M. Chen, and Y. Li, "Alignment calibration of IMU and Doppler sensors for precision INS/DVL integrated navigation," *Optik*, vol. 126, no. 23, pp. 3872–3876, 2015.

[8] W. Li, L. Yang, L. Zhang, M. Chen, and K. Tang, "A robust method for alignment calibration of an inertial measurement unit (IMU) and Doppler sensors," *Lasers in Engineering*, vol. 34, pp. 93–106, 2016.

[9] L. Chang, Y. Li, and B. Xue, "Initial alignment for a Doppler Velocity Log-aided Strapdown Inertial Navigation System with limited information," *IEEE/ASME Transactions on Mechatronics*, vol. 22, no. 1, pp. 329–338, 2016.

[10] "Workhorse navigator Doppler Velocity Log (DVL) ," 2013, http://www.teledynemarine.com/Lists/Downloads/navigator_datasheet_lr.pdf.

[11] L. Zhao, X. Liu, L. Wang, Y. Zhu, and X. Liu, "A pretreatment method for the velocity of DVL based on the motion constraint for the integrated SINS/DVL," *Applied Sciences*, vol. 6, no. 79, 2016.

[12] Q. Wang, X. Cui, Y. Li, and F. Ye, "Performance enhancement of a USV INS/CNS/DVL integration navigation system based on an adaptive information sharing factor federated filter," *Sensors*, vol. 17239 pages, 2017.

[13] Y. Yao, X. Xu, Y. Li, and T. Zhang, "A hybrid IMM based INS/DVL integration solution for underwater vehicles," *IEEE Transactions on Vehicular Technology*, vol. 68, no. 6, pp. 5459–5470, 2019.

[14] P. Liu, B. Wang, Z. Deng, and M. Fu, "INS/DVL/PS tightly coupled underwater navigation method with limited DVL measurements," *IEEE Sensors Journal*, vol. 18, no. 7, pp. 2994–3002, 2018.

[15] D. Wang, X. Xu, Y. Yao, T. Zhang, and Y. Zhu, "A novel SINS/DVL tightly integrated navigation method for complex environment," *IEEE Transactions on Instrumentation and Measurement*, In press, 2019.

[16] R. Eliav and I. Klein, "INS/Partial DVL measurements fusion with correlated process and measurement noise," in *Proceedings of 5th International Electronic Conference on Sensors and Applications*, vol. 4, Amsterdam, Netherlands, November 2019.

[17] T. Yoo, M. Kim, S. Yoon, and D. Kim, "Performance enhancement for conventional tightly coupled INS/DVL navigation system using regeneration of partial DVL measurements," *Journal of Sensors*, vol. 2020, Article ID 5324349, 15 pages, 2020.

[18] A. Tal, I. Klein, and R. Katz, "Inertial navigation system/Doppler velocity log (INS/DVL) fusion with partial DVL measurements," *Sensors*, vol. 17, no. 415, 2017.

[19] Y. Zhu, X. Cheng, J. Hu, L. Zhou, and J. Fu, "A novel hybrid approach to deal with DVL malfunctions for underwater integrated navigation systems," *Applied Sciences*, vol. 7, no. 759, 2017.

[20] Z. Wu and W. Wang, "INS/magnetometer integrated positioning based on neural network for bridging long-time GPS outages," *GPS Solutions*, vol. 23, no. 3, 88 pages, 2019.

[21] G. Wang, X. Xu, Y. Yao, and J. Tong, "A novel BPNN-based method to overcome the GPS outages for INS/GPS system," *IEEE Access*, vol. 7, pp. 82134–82143, 2019.

[22] Y. Yao, X. Xu, C. Zhu, and C.-Y. Chan, "A hybrid fusion algorithm for GPS/INS integration during GPS outages," *Measurement*, vol. 103, pp. 42–51, 2017.

[23] Q. Y. Wang, K. Liu, Z. Sun, and M. Zhang, "Research into the high-precision marine integrated navigation method using INS and star sensors based on time series forecasting BPNN," *Optik*, vol. 172, pp. 494–508, 2018.

[24] E. Cadenas, W. Rivera, R. Campos-Amezcua, and C. Heard, "Wind speed prediction using a univariate ARIMA model and a multivariate NARX model," *Energies*, vol. 9109 pages, 2016.

[25] Z. Boussaada, O. Curea, A. Remaci, H. Camblong, and N. Mrabet Bellaaj, "A nonlinear autoregressive exogenous (NARX) neural network model for the prediction of the daily direct solar radiation," *Energies*, vol. 11620 pages, 2018.

[26] L. Wang, L. Fu, and M. Xin, "Sculling compensation algorithm for SINS based on two-time scale perturbation model of inertial measurements," *Sensors*, vol. 18282 pages, 2018.

[27] Z. Ye and M. K. Kim, "Predicting electricity consumption in a building using an optimized back-propagation and Levenberg-Marquardt back-propagation neural network: case study of a shopping mall in China," *Sustainable Cities and Society*, vol. 42, pp. 176–183, 2018.

[28] W. Li, W. Wu, J. Wang, and M. Wu, "A novel backtracking navigation scheme for autonomous underwater vehicles," *Measurement*, vol. 47, pp. 496–504, 2014.